

# PlumeViz: Interactive Exploration for Multi-Facet Features of Hydrothermal Plumes in Sonar Images

Yiming Shao, Chengming Liu, Zhiyuan Meng, Shufan Qian, Peng Jiang, Yunhai Wang, Qiong Zeng

## ABSTRACT

Plume visualization is essential for unveiling the dynamics of hydrothermal systems. This paper introduces an interactive exploration tool, PlumeViz, designed to facilitate the extraction and visualization of multifaceted plume characteristics from the COVIS datasets. The tool addresses the challenges posed by undersampled volume data and intricate plume structures by providing an interactive platform for plume identification, quantification, and visual representation. Key functionalities of PlumeViz encompass comprehensive plume evolution, plume feature extraction, and in-depth exploration of specific regions of interest. We demonstrate the efficacy of PlumeViz in visualizing hydrothermal plumes through a case study and a range of illustrative results.

**Keywords:** Sonar imaging for hydrothermal plumes, scientific visualization

## 1 INTRODUCTION

Submarine plumes serve as essential markers for researchers studying deep-sea hydrothermal systems. Acoustic imaging methods are developed to detect hydrothermal discharges via data with many different facets, such as plume imaging and plume velocity. Visualization techniques play a significant role in analyzing such data. However, due to the undersampled volume and the high dynamic range of volume data in time sequences, it is cumbersome and inaccurate to detect and visualize plumes. Therefore, we propose an interactive system for users to analyze such data and explore multi-facet features with user-interested visual encodings.

## 2 APPROACH

Our interactive exploration tool incorporates three key functionalities, including dynamic plume evolution, multi-facet plume feature extraction, and region-of-interest exploration. The dynamic plume evolution visualizes temporal changes in plume bending and structure, while the multi-facet plume feature extraction displays various plume characteristics such as plume centerline, backscatter intensity gradients, and heat flux. The region-of-interest exploration enables scientists to examine different plume candidates and modify visual encodings for in-depth analysis. We will detail each functionality in this section.

### 2.1 Dynamic Plume Evolution

A primary goal of our tool is to support an overview visualization of plume changes. Our input dataset consists of 3D plume images interpolated onto a uniform rectangular grid. By extending the region-growing algorithm [1] to gridded temporal volume data, we can segment the data into multiple, independent regions representing continuous hydrothermal plume candidates in the spatiotemporal domain. We hypothesize that regions with more voxels are more likely to be plumes. Accordingly, our system identifies potential plumes based on voxel counts and associated uncertainties. The region with the highest voxel count is initially displayed as the default plume.

A challenge in visualizing dynamic changes is the undersampling of the provided temporal sequence. To facilitate smooth data evolution, we interpolate data between consecutive time steps using linear interpolation. We then visualize the temporal plumes through classic

ray casting volume rendering, employing a carefully designed color and a log-scaled opacity transfer function. To ensure consistent comparability of rendered plume values across different time steps, we apply a single colormap to all data, allocating more colors to data ranges with higher value frequencies.

### 2.2 Multi-Facet Plume Feature Extraction

Our second aim is to provide insights into plume behavior through multi-faceted plume feature extraction. Visualizing and quantifying key characteristics, such as plume centerlines, backscatter intensity gradients, and heat flux, can help researchers uncover essential information about plume trajectory, internal structure, and thermal impact.

#### 2.2.1 Plume Centerline

We extract the plume centerline and calculate its curvature to quantify plume bending and degree. Specifically, we first identify the line connecting points of maximum concentration within each plume cross-section along the z-axis [3]. These connecting points are then fitted with a smooth quadratic polynomial function,  $g(x) = ax^2 + bx + c$ , where the unknown parameters are optimized using the least mean squared error:

$$P(a, b, c) = \min \sum_{i=1}^m (g(x_i) - y_i)^2, \quad (1)$$

where  $m$  is the number of connecting points,  $y_i$  is the corresponding value of the  $i$ -th point, and  $g(x_i)$  is the estimated value of  $x_i$  under the parameter set  $(a, b, c)$ . Based on the fitted centerline function, we can calculate the curvature of the centerline along the z-axis to measure the degree of its bending.

#### 2.2.2 Backscattering Intensity Gradients

To analyze plume intensity and direction changes, we calculated backscattering intensity gradients using central differences, with a default step size  $h = 1$ :

$$\nabla f(x, y, z) \approx \frac{1}{2h} \begin{pmatrix} f(x+h, y, z) - f(x-h, y, z) \\ f(x, y+h, z) - f(x, y-h, z) \\ f(x, y, z+h) - f(x, y, z-h) \end{pmatrix}. \quad (2)$$

These gradients can be visualized as either small arrows or streamlines. Our tool employs the classic fourth-order Runge-Kutta algorithm for streamline generation. To produce high-quality streamlines, careful seed point selection is necessary. Given the importance of the centerline in revealing plume structures, we propose a strategy. Initially, equidistant points were selected along the centerline, followed by random sampling of seed points in their vicinity.

#### 2.2.3 Dynamic Hydrothermal Discharges

**Vertical Velocity.** To address the need for research on plume dynamics and energy, we require a comprehensive analysis and visualization of Doppler data. The initial step involves calculating the plume velocity from the Doppler measurements. We first identify target plume regions using the method outlined in Section 2.1. In accordance with the “dominant eddy” concept [2], fluid velocities within this region are heavily influenced by the centerline velocities

of the plume. Consequently, following the processing workflow described in [5], we extract the plume centerline velocity from the Doppler data and combine it with the line-of-sight velocities at all points within the plume region to compute the complete plume velocity. By visualizing the velocity strength with a classic ray casting algorithm and the velocity streamlines generated with the fourth-order Runge-Kutta method, we demonstrate the tool's capability to support hydrodynamic plume studies. Note that the z-component of the calculated velocity represents the vertical plume velocity, which will be used to determine plume heat flux in the subsequent section.

**Heat Flux.** Heat flux is an important factor to study the dynamic hydrothermal discharges in vertical directions. We follow the method described in [5] and [6] to calculate heat flux from the plume doppler velocity data. For each extracted plume region, we get velocity information on the centerline [5], which in turn interpolates the velocity field of the plume region. Based on the plume velocity field, we can calculate heat flux of the plume using the classic formula from the plume buoyancy [6]. In this method, the connection between heat flux and buoyancy is depicted as the equation below:

$$H_x = \frac{c_p \rho_{ref}}{g \alpha_T} B_x, \quad (3)$$

where  $H_x$  and  $B_x$  refer to the heat flux and buoyancy at the plume vent, respectively. The buoyancy at the plume vent is equal to the integral of the vertical velocity at the vent multiplied by a factor consisting of the plume initial density  $\rho_x$ , seawater density  $\rho_w$ , reference density  $\rho_{ref}$ , and gravity acceleration  $g$ :

$$B_x = \int_{A_x} W_x g (\rho_w - \rho_x) / \rho_{ref} dS, \quad (4)$$

where  $x$  is any coordinate in space,  $A_x$  is unit area at coordinate  $x$ . We refer readers to prior literature [5] and [6] for a complete review of the heat flux calculation process. We leverage the classic ray casting algorithm to render the calculated heat flux strengths with a *coolwarm* colormap and a log-scaled opacity function.

### 2.3 Interactive Exploration

Our interactive tool offers flexibility for both exploring specific plume regions and examining different plume structures. Users can select regions of interest and adjust rendering settings as needed.

**Region-of-Interest Selection.** Given the extensive range of plume imaging data and noise present in extracted plume regions, we offer both cropping and region selection tools to facilitate user exploration. The cropping tool enables users to define the desired area by adjusting axis sliders, with the 3D crop displayed dynamically. For more focused analysis, the region selection tool allows users to pinpoint specific plume regions by clicking on corresponding areas within a 2D navigation map.

**Parameter Control.** Our tool integrates a diverse range of continuous color maps from Python's Matplotlib library. Users can choose their preferred color maps, and our tool will automatically adjust the color distribution to align with the data distribution. Additionally, users have the flexibility to modify the opacity function to enhance the visualization of the inner plume structures of interest. We also provide interfaces that allow users to specify values for extracting isosurfaces from the 3D plume imaging data.

## 3 RESULTS

We implemented our tool using Python, leveraging QT for interface development and VTK [4] for part of the visualizations. Our PlumeViz tool is available at <https://github.com/syming123/plumeviz>.

### 3.1 Case Study

Before delving into in-depth analysis, users are drawn to a visually appealing overview. Figure 1 presents a comprehensive overview of hydrothermal plume sonar imaging data, organized in a clear and aesthetically pleasing manner. By interactively selecting a plume region of interest on the navigation map, users can explore the plume's multifaceted characteristics across different time steps.

Figure 2 showcases the temporal changes in plume shape and centerline bending structure using a combination of direct and indirect volume rendering techniques. Comparing plume regions at various time steps reveals the evolution of internal structures and the diffusion process.

To further demonstrate the horizontal dispersion of the plume, we present streamlines derived from the backscatter intensity gradient field in Figure 3. Finally, to understand the dynamic hydrothermal discharges, vertical velocity streamlines and heat flux values are presented in Figure 4.

### 3.2 Evaluation with Domain Experts

We conducted informal interviews with two marine geologists. One had 20 years of experience researching submarine hydrothermal fluids and plumes, while the other had 18 years of experience focused on marine geochemistry and petrology. Both experts expressed enthusiasm for our tool's capacity to generate high-quality visualizations of hydrothermal plumes. They found it straightforward to identify plume regions and observe distinct plume patterns. Both scientists expressed appreciation for our work and indicated an interest in potential collaborations. While one scientist expressed interest in visualizing small eddies within plumes, this is currently beyond the capabilities of our tool due to limitations in sonar imaging resolution. We aim to address this in future work.

## 4 CONCLUSION

We introduced an interactive exploration tool for visualizing dynamic hydrothermal plumes in sonar imaging. Our results effectively demonstrate plume bending, structure, and temporal changes. Equipped with region-of-interest selection and parameter controls, our tool empowers users to investigate diverse plume features, including bending direction and degree, backscattering intensity gradients, and dynamic hydrothermal discharges.

## REFERENCES

- [1] K. G. Bemis, D. Silver, G. Xu, R. Light, D. Jackson, C. Jones, S. Ozer, and L. Liu. The path to covis: A review of acoustic imaging of hydrothermal flow regimes. *Deep Sea Research Part II: Topical Studies in Oceanography*, 121:159–176, 2015. Exploring New Frontiers in Deep-Sea Research: In Honor and Memory of Peter A. Rona. 1
- [2] V. H. Chu. Lagrangian scaling of turbulent jets and plumes with dominant eddies. In *Recent research advances in the fluid mechanics of turbulent jets and plumes*, pp. 45–72. Springer, 1994. 1
- [3] P. A. Rona, K. G. Bemis, D. Silver, and C. D. Jones. Acoustic imaging, visualization, and quantification of buoyant hydrothermal plumes in the Ocean. *Marine Geophysical Research*, 23(2):147–168, Jan. 2002. 1
- [4] W. Schroeder, K. M. Martin, and W. E. Lorensen. *The visualization toolkit (2nd ed.): an object-oriented approach to 3D graphics*. Prentice-Hall, Inc., USA, 1998. 2
- [5] G. Xu, D. Jackson, K. Bemis, and P. Rona. Observations of the volume flux of a seafloor hydrothermal plume using an acoustic imaging sonar. *Geochemistry, Geophysics, Geosystems*, 14(7):2369–2382, 2013. 2
- [6] G. Xu, D. R. Jackson, K. G. Bemis, and P. A. Rona. Time-series measurement of hydrothermal heat flux at the grotto mound, endeavour segment, juan de fua ridge. *Earth and Planetary Science Letters*, 404:220–231, 2014. 2

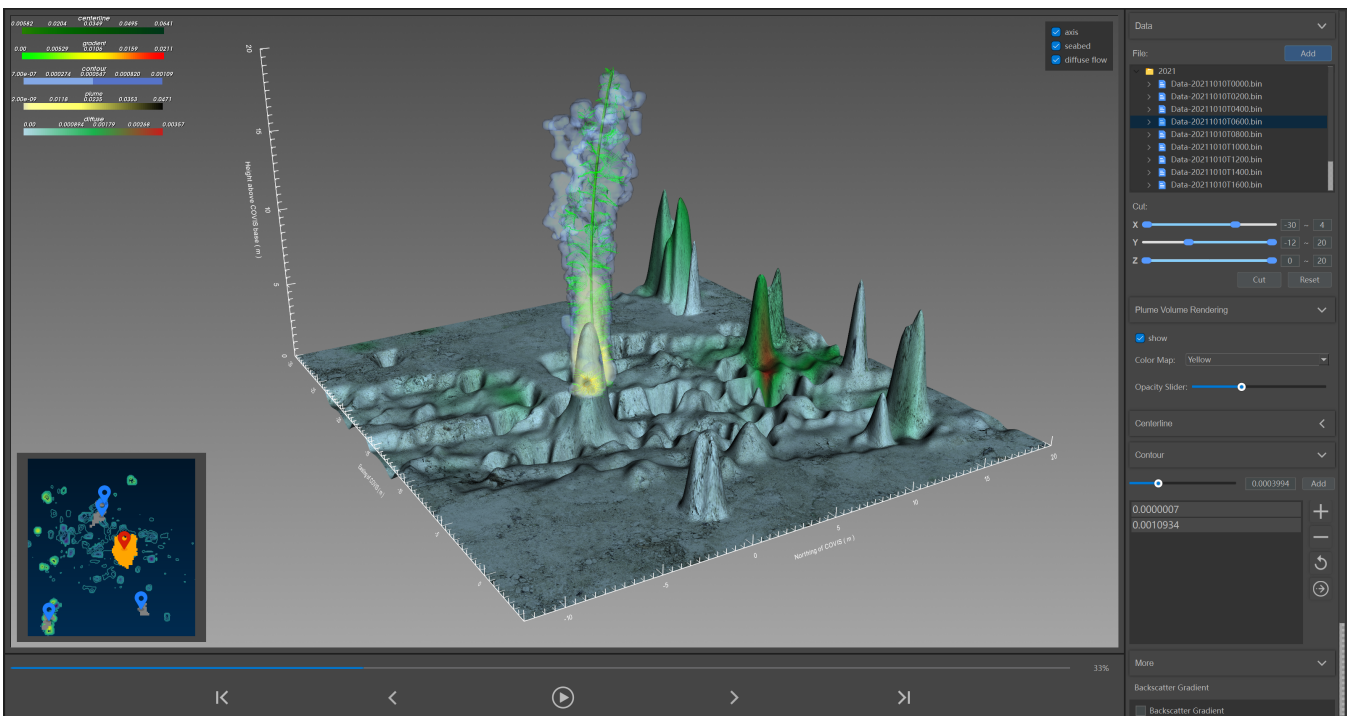


Figure 1: PlumeViz interface showcasing an overview visualization of multi-faceted plume characteristics. These include a 3D plume structure, centerline, and backscattering intensity gradients, in addition to seafloor topography and diffuse flow patterns.

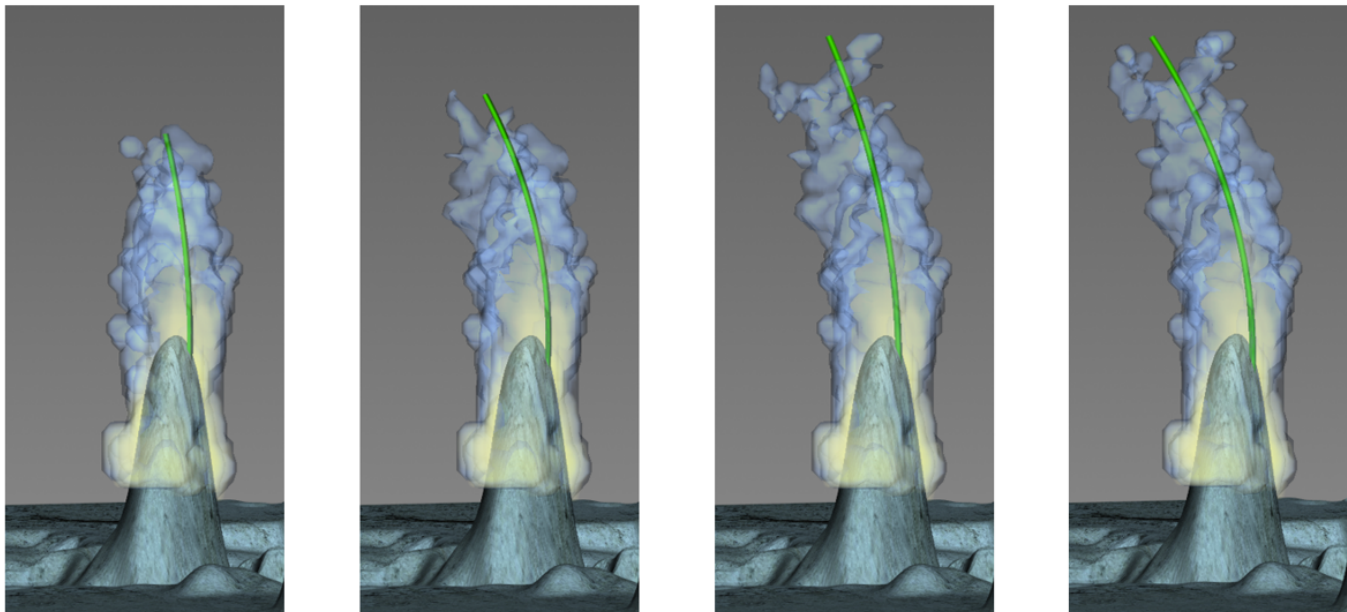


Figure 2: Temporal evolution of plume shape and centerline bending structure on August 16th, 2020, visualized from left to right using a combination of direct and indirect volume rendering techniques. In this figure, the yellow colors indicate plume intensities, with higher opacities corresponding to greater values. The blue surface delineates a specific value of interest to the domain expert. The plume centerline is depicted by the green curve.

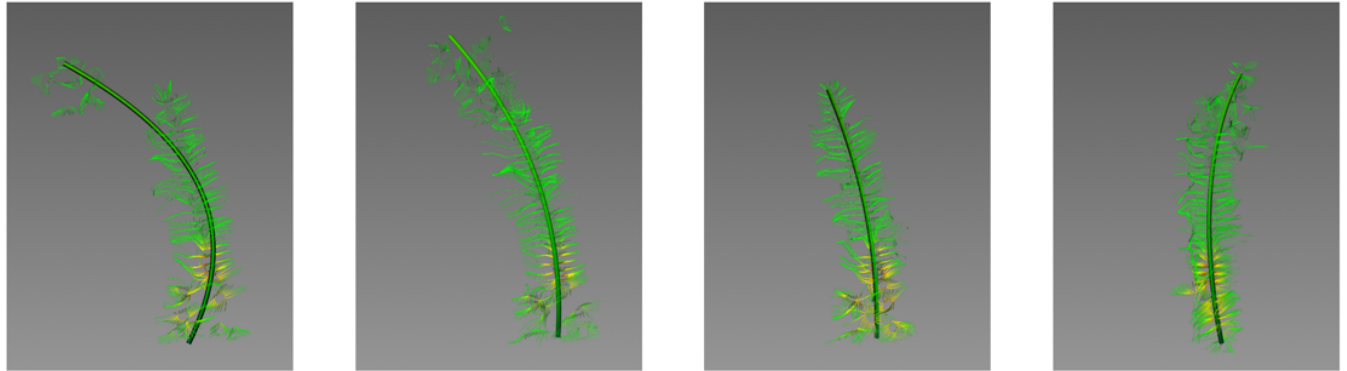


Figure 3: Temporal changes of the plume's centerline on August 16th, 2020, illustrated alongside the streamlines of the backscattering gradient.

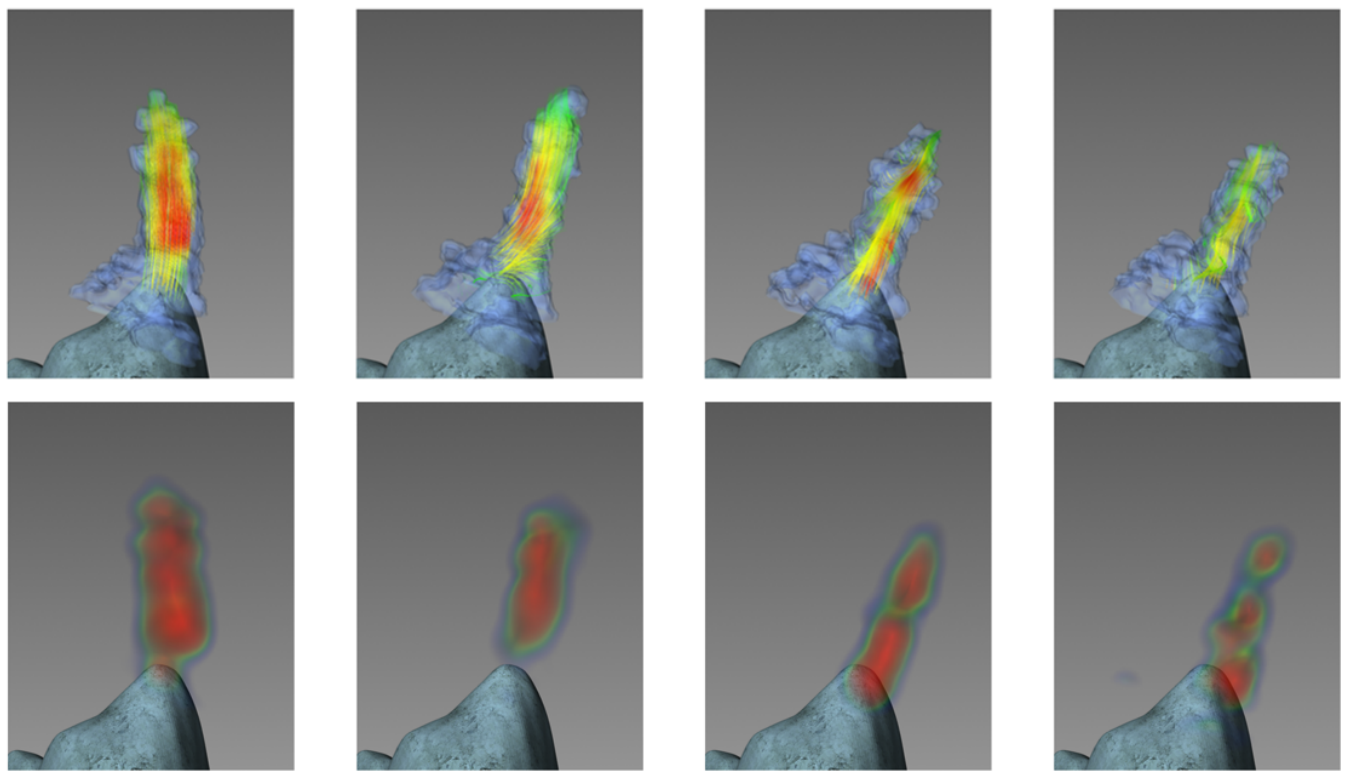


Figure 4: Temporal changes in the vertical velocity of the plume are depicted in the top row, with the corresponding heat flux illustrated in the bottom row, both measured on October 8th, 2014.